

# The investigation of ultrasonic fields by time resolved X-ray diffraction

K.-D. Liss<sup>a</sup>, A. Magerl<sup>b</sup>, R. Hock<sup>c</sup>, B. Waibel<sup>d,e</sup>, A. Remhof<sup>e</sup>

<sup>a</sup>European Synchrotron Radiation Facility, B.P. 220, F-38043 Grenoble Cédex

<sup>b</sup>Lehrstuhl für Kristallographie und Strukturphysik, Universität Erlangen Nürnberg, D-91054 Erlangen

<sup>c</sup>Mineralogisches Institut der Universität Würzburg, Am Hubland, D-97074 Würzburg

<sup>d</sup>Institut Max von Laue — Paul Langevin, B.P. 156, F-38042 Grenoble Cédex

<sup>e</sup>Ruhr-Universität Bochum, D-44780 Bochum

## ABSTRACT

Time resolved detection in both detector and synchrotron resolution mode are presented. Using this technique the response of the Bragg profile in perfect Silicon to a MHz ultrasonic wave field has been studied on the high resolution triple crystal diffractometer at the ESRF high energy beamline ID15A. High photon energies up to 500 keV have been used for the analysis of a longitudinal acoustic wave in the 10 mm bulk. First, conventional time averaged rocking curves show intensity gains by up to a factor of 50, and a reciprocal space mapping reveals full information on the acoustic wave vector. Secondly, time and space resolved reflection curves have been taken. They give detailed insights into the properties of the acoustic wave field in space and time. In particular, they allow us to identify uniquely true standing waves without parasitic strain components or higher harmonic excitation. Time averaged and snapshots of the time resolved rocking curves represent different aspects of the density of states for the lattice parameter distribution. They are understood analytically by the elliptic integral K and the inverse circle function, respectively.

**Keywords:** sub-nanosecond time resolution; synchrotron bunches; ultrasound acoustics; high energy X-rays; high resolution diffractometer;

## 1. INTRODUCTION

Crystals subjected to ultrasonic excitations have been investigated for some time by X-ray and neutron diffraction methods. Fundamental questions such as the investigation of the diffraction process itself as a response to the ultrasonic field as well as its applications to beam optics or materials research are of interest. The first X-ray diffraction experiments on oscillating crystals were performed in 1931<sup>1</sup> stimulating large discussion to explain the observed increase in intensity of the Laue spots. Neutron experiments go back to the 60's<sup>2</sup>. Nowadays the scientific community still treats ultrasonically excited crystals in short wavelength diffraction. Applications from focusing effects<sup>3</sup>, monochromators with tunable bandwidths<sup>4,5</sup>, the characterization of static but tiny strain fields<sup>6,7</sup> have been discussed as well as fundamental questions about the formation of satellites<sup>8</sup> and its applications, inter-branch scattering, gradient crystal effects and the fundamental difference between neutron- and X-ray diffraction found their audience<sup>5</sup>. Theoreticians have tried to explain the variety of effects and have predicted even more challenging fields for experimentalists, like, for example, the formation of caustics in Laue diffraction<sup>9</sup>. The studies above all involve the spatial characteristics, but also attempts to investigate the temporal parameter have been made earlier in special cases of X-ray<sup>10</sup> and neutron diffraction<sup>11</sup>. Some work has been carried out with modulated ultrasonic waves<sup>12,13,14,15</sup> impregnating an artificial time structure to the carrier wave. Systematic investigation of the ultrasonic wave directly became possible only with the brilliance and the penetration of high energy synchrotron sources<sup>16</sup>. Additionally the time structure of these sources allow the step from a nanosecond to a sub-nanosecond resolution down by an order of magnitude which generally is a challenging domain in solid state physics.

## 2. THE DIFFRACTOMETER AND TIME RESOLVED DETECTION

The experiments described in this article have all been performed on the high resolution triple axis diffractometer at the high energy beamline ID15A of the ESRF. Basically it works in a non dispersive setup, the rotation axes of the monochromator, sample and analyzer being controlled by optical interferometers. Angles are controlled relatively to an accuracy of 0.1" which

---

Further author information —

Email: liss@esrf.fr — WWW: [http://www.esrf.fr/exp\\_facilities/id15a/people/liss/Liss.html](http://www.esrf.fr/exp_facilities/id15a/people/liss/Liss.html)

corresponds to about  $\Delta G_{\parallel}/G = 5 \cdot 10^{-6}$  and  $\Delta G_{\perp}/G = 5 \cdot 10^{-7}$  for longitudinal and transverse resolution, respectively. A more detailed description and a strategy of reciprocal space mapping for crystals without mosaic spread is given in a recent publication<sup>17</sup> and has been employed on ultrasonically excited crystals as described in<sup>16</sup>. High energies between 85 keV and 500 keV were used for the high penetration power through a 10 mm thick silicon sample and partly for fulfilling kinematical conditions.

The time resolved feature has been developed with the series of experiments leading to the present publication. It was constantly improved and now can be considered as a standard option of the instrument. First the time resolution of the germanium detector itself was used with a 20 ns resolution operating independently from the time structure of the synchrotron mode. After very successful results the time resolution was improved by two orders of magnitude down to about 200 ps by taking advantage of the 16-bunch mode of the storage ring. Schematic diagrams for the detection electronics and the corresponding signals are given in figures (1) and (2) for detector and synchrotron resolution, respectively. In both cases a slow and a fast channel for good energy and maximum time resolution are brought to coincidence. The signal of the 3 cm thick by 3 cm diameter coaxial germanium detector, a negative raising edge of about 100 ns with a slow exponential decrease of the created charge, is split into a fast and a slow channel for time and energy resolution, respectively.

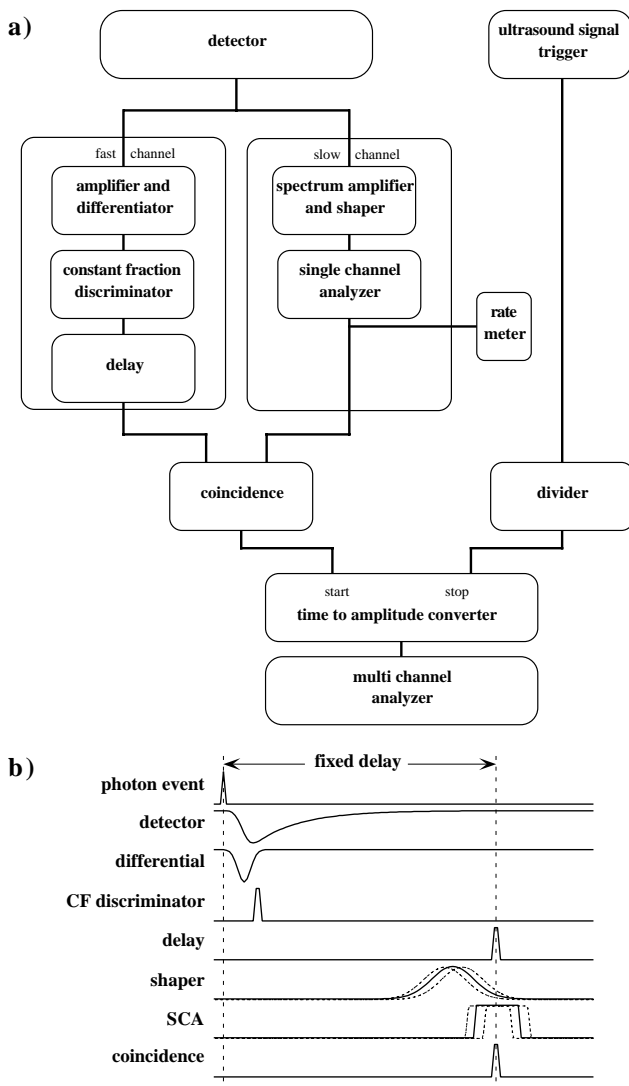


Figure 1: Block diagram a) and qualitative signal pulse diagrams b) of the detector electronics using its intrinsic time resolution. The detector signal is split into a time resolving fast channel and an energy discriminating jittering slow channel, its coincidence starting the clock, the time to amplitude converter. Stop signals are obtained from the ultrasound phase trigger which can be divided to record multiple periods.

The energy resolving slow channel consists of the standard spectrum amplifier and shaper with a Gaussian pulse output, its amplitude being proportional to the total charge created, i.e. the photon energy. A single channel analyzer discriminates the interesting energy by the pulse amplitude and a rectangular output signal is created when the photon energy falls into the window set. Charge integration and discrimination occur on the  $\mu$ s or just sub- $\mu$ s scale and thus reveals a large jitter in time of about 50 ns to 100 ns. This number holds for a monochromatic beam and increases largely when photons of different energies are investigated.

In the detector resolution case the fast channel is triggered to the negative raising edge of the detector pulse itself which then decreases slowly towards its zero count rate voltage. To remove that constant offset which even shifts with higher count rates the signal is differentiated, basically by a condenser or now by a more sophisticated module card. The trigger point is obtained best by a constant fraction discriminator, a standard module in time resolved applications which takes the input pulse, adds to it its own negative value but delayed in time, thus producing a bi-polar pulse with a central zero transition, the trigger point, independent of the original pulse height which depends on the photon energy. Now coincidence is taken by the slow and the fast channel, the latter being delayed by an appropriate device to coincide with the slower output.

The fast channel provides a signal each time a photon arrives while the slow channel gives an event only when this photon falls into the correct energy range, thus the coincidence output delivers the time when the right photon arrives, with a fixed time offset from the moment when the photon was really detected or scattered at the sample.

In the time resolving synchrotron mode  $N=16$  or less bunches are distributed uniformly around the storage ring. Out of 992 bunch positions only every 992/ $N$ -th position is filled while all others are suppressed by  $10^{-6}$  or better. A bunch packet lasts typically 100 ps and the arrival time is known very accurately relative to the bunch clock. Consequently the X-ray photons arrive in well defined flashes and possible arrival

times at the detector or sample are strongly related to the phase of the bunch clock. Thus the slow channel superimposed in time with a tick of the bunch clock – which tick does not matter, because the bunch clock is a clock, i.e. a device which counts the time – accurately delivers the time of the scattering event but with a phase factor.

To resume, the bunch clock delivers the time when a scattering process may occur while the slow detector channel tells whether a photon with the right energy has arrived, their coincidence giving the event with the corresponding time.

In both time resolution modes the coincidence signal starts a clock, the time-to-amplitude-converter which is then stopped by the trigger signal of the ultrasonic wave excitation, i. e. the remaining time from the photon event to the zero transition, but a phase is measured. This inverse mode is chosen since detector events occur much less often than trigger points of the 10 MHz ultrasonic wave and results in a negative time axis of the multi channel analyzer. The latter sorts event pulses according to their heights which are proportional to the time difference between the stop and the start impulse of the time-to-amplitude-converter. Stroboscopic repetition occurs until statistics are satisfied.

The time resolution can be tested by measuring the synchrotron filling itself. Therefore, the stop signal is triggered to the bunch clock. Figure (3) shows the fill of the ESRF hybrid mode, where 1/3 of the 992 bunches are filled continuously and a stronger opposite single bunch separates the empty 2/3. This mode is used for beamlines like ID9<sup>18</sup> which operate with the time resolution of the single bunch alone while the large current of the 1/3 fill is available for all standard time integrating instruments. The width at half maximum of 20 ns of the single bunch, which physically is about 100 ps narrow, shows in an easy way the time resolution of the detector mode. For completeness, note the four 10 % oscillations in the 1/3 fill which first were considered as noise in the system but which could not be removed by adjusting the electronics. It turned out that this oscillation was real when the control room of the machine was asked, the signal being confirmed by their own investigation.

Of course, hybrid mode cannot be used in the synchrotron time resolution mode described, and figure (4) shows the structure in the ESRF 16 bunch mode. Neighboring X-ray flashes are separated by 176 ns and last physically no longer than 100 ps. The full widths at half maximum evolve from 167 ps at 36 ns, 235 ps at 212 ns towards 362 ps after 388 ns while the integrated intensity in each flash remains constant at about 114000 counts per 88 s. The larger time jitter for longer time measurements is due to both the accuracy of the time-to-amplitude converter and the multi channel analyzer and is about 0.1% of the total time passed between the start and the stop signal.

Concluding with this chapter, two modes for time resolution are operational on ID15A, the detector and the synchrotron mode with 20 ns and about 200 ps full width at half maximum, respectively. Note that these modes are applicable when the scattering process is instantaneous rather than, for example, in nuclear resonance spectroscopy, and a repetitive oscillation of the sample is studied. Also an avalanche diode with a sub-ns resolution was tested but the efficiency for 100 keV X-rays was below  $10^{-3}$ .

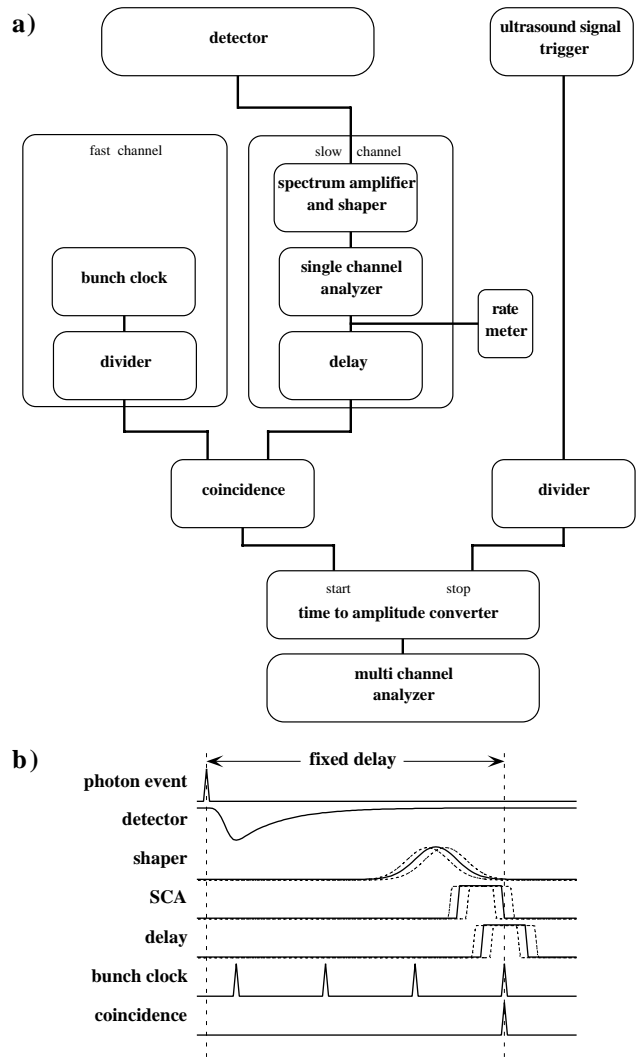


Figure 2: Similar diagrams to Figure (1) but for time resolution in the synchrotron mode. The fast channel is replaced by the signal from the bunch clock.

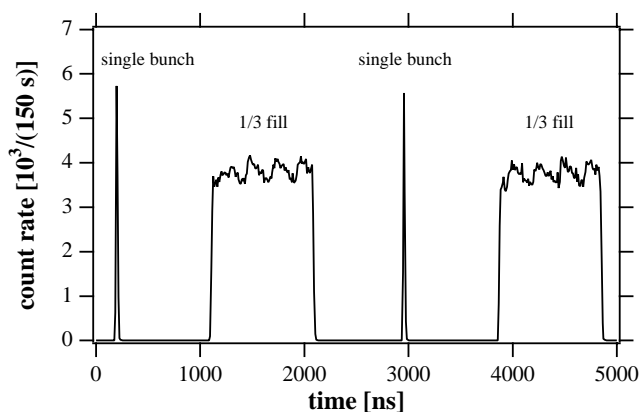


Figure 3: Time structure of the storage ring in hybrid mode. A single bunch of 5 mA is opposite to a 1/3 fill of continuous bunches. The single bunch can be used to measure the time resolution of our instrument. Here its breadth is 20 ns, the value for the germanium detector at fixed energy. The 10 % oscillations on top of the 1/3 fill are real and have been confirmed by the control room. The time scale is negative, earlier moments in time being on the right.

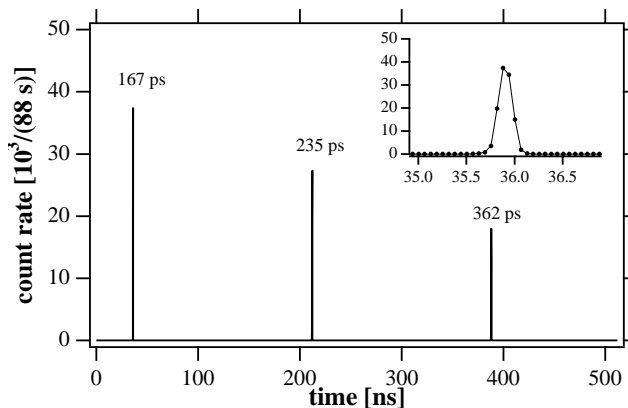


Figure 4: X-ray pulses in the 16 bunch mode of the storage ring being separated by 176 ns. The insert shows a magnification of the first peak. The spectrum allows to calibrate the time resolution of the system which evolves from 167 ps to 362 ps due to the accuracy of the time-to-amplitude converter. As before, the time scale is negative.

### 3. ULTRASONIC WAVES SETUP

Hard X-ray diffraction on ultrasonically excited silicon crystals has been studied at ID15A since 1995, always using very similar set-ups. Details of the time integrated response can be found in <sup>16</sup>. The brilliance of the new source and the high energy range with the ultimate instrument resolution open new fields of investigation never possible before. A short introduction to the time resolved studies is published in <sup>19</sup> and related information is found on the internet <sup>20</sup> while the present paper tends to treat more completely the wide range of effects observed.

The experimental situation is presented in figure (5). A 10 mm thick perfect silicon crystal, 30 mm × 30 mm large, is excited into acoustic vibrations by a lithium niobate transducer coupled to one of its plane parallel (111) surfaces. Overtone polished transducers with 2.5 MHz or 5 MHz ground eigen-frequencies were used and the electrical exciting frequency could be varied between zero and 20 MHz. Firstly the -351 diffraction planes in asymmetric Laue geometry were chosen <sup>16</sup> and are inclined by 73° towards the sound vector. In this way one integrates diffracted intensity from the whole crystal thickness, in particular over several acoustic wavelengths. The standing, longitudinal acoustic wave consists of regions with an

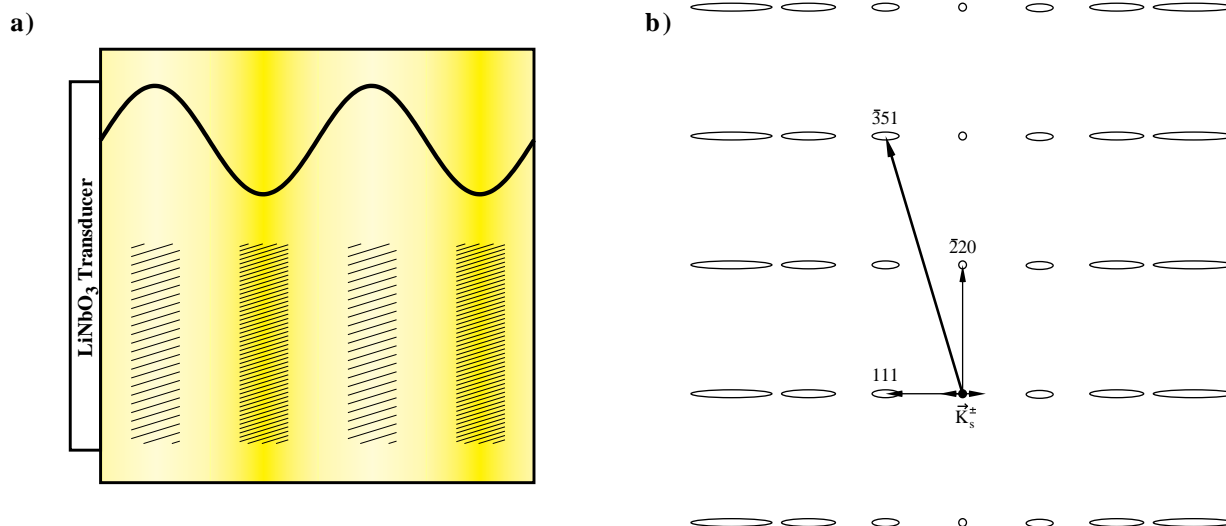


Figure 5: Geometrical setup for the ultrasonically excited silicon crystal in real space, a) and reciprocal space, b). Compressional ultrasonic waves in the MHz range are excited by a LiNbO<sub>3</sub> transducer in the 111 direction of a 10 mm thick silicon crystal. Regions of compressed and expanded lattice parameters vary as a function of time with gradients expanding the reciprocal lattice points in the direction of the sound vector. In particular, we measured the -351 reflection in asymmetric Laue geometry which is inclined by 73° to the 111 direction.

expanded and others, half a wavelength further, with a compressed lattice parameter, interchanging half a period in time later. These momental strain fields cause lattice parameter gradients resulting in a broadening of the reflection curve.

The sample was mounted onto the second axis of the triple axis diffractometer operating in high resolution mode<sup>17</sup>. An equivalent monochromator reflection was employed to work perfectly in non-dispersive geometry. Optionally, a similar analyzer crystal can be used for reciprocal space mapping. The experimental situation is sketched in figure (5b). Reciprocal lattice points, originally dots, elongate along the [111] direction which has been confirmed experimentally in the cited paper<sup>16</sup>. Rocking scans in two axes mode, by tuning the sample against the fixed monochromator, integrate over the longitudinal diffraction component but are still convenient for perfect crystals without mosaic spread, because fast<sup>17</sup>. Figure (6) shows a series of rocking curves as a function of a voltage parameter proportional to the ultrasonic amplitude. The frequency is 15.544 MHz operating in the third overtone harmonics of the 5 MHz transducer, and an X-ray energy of 90 keV with a Pendellösung period of 393 μm was chosen for these measurements. The narrowest curve, a Lorentzian corresponding to the unexcited sample has a width of 0.2" which truly is the folded value given by dynamical theory of diffraction. As soon as one applies lattice strain by the exciting voltage, the intensity doubles and a plateau broadening the reflection curve forms by increasing the strain. This is understood since intensity in a perfect crystal competes by the Pendellösung effect between the forward and Bragg diffracted direction and results in a 50% – 50% solution for a thick sample. This Pendellösung effect is lost by the tiniest gradient where all intensity goes in favor for the Bragg diffracted reflection<sup>21</sup>. Peak intensity drops from one when the crystal tends to scatter kinematically for highest excitation voltages. Atomic amplitudes of 210 Å peak to peak could be deduced from the behavior of the wings of the rocking curves<sup>16</sup>.

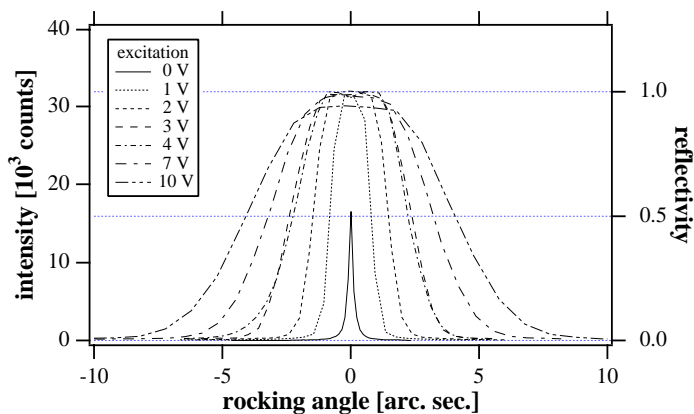


Figure 6: Rocking curves as a function of ultrasonic excitation proportional to the voltage parameter shown. The unexcited crystal reflects the central Lorentzian with a full width of half maximum of 0.2 arc. sec. corresponding to dynamical theory of reflection. In the Laue case its peak reflectivity is 50% in contrast to 100% for a weak gradient crystal.

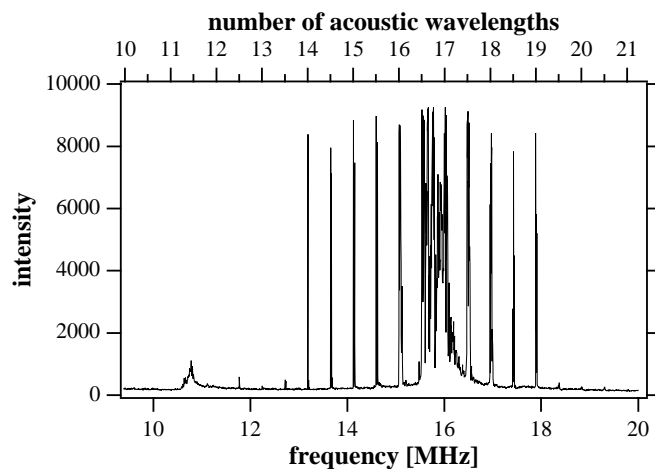


Figure 7: Acoustic resonances for the 10 mm thick crystal and a 5 MHz transducer. The large resonance distribution around 16 MHz and the small but broad peak at 10.7 MHz correspond to the 3<sup>rd</sup> and forbidden 2<sup>nd</sup> transducer harmonics, respectively. The sharp resonances between 13 MHz and 18 MHz are due to a standing wave field in the silicon only. The number of wavelength in the crystal is shown on the top axis.

Figure (7) shows an acousto-mechanic resonance spectrum. For its measurement, the rotation of the sample has been positioned about 1" besides the maximum of the unexcited crystal curve. Therefore only high intensity gets scattered when the rocking curve broadens due to the sample getting into resonance making large atomic amplitudes and thus large lattice parameter gradients present. The frequency scan goes from 9.7 MHz to 20 MHz showing a large resonance, the 3<sup>rd</sup> transducer harmonics around 16 MHz. Further more the quasi forbidden 2<sup>nd</sup> harmonic is found at 10.7 MHz while a large number of sharp silicon resonances appear, mainly between 12.5 MHz and 18 MHz being only about 1 kHz large. Since the rocking curves for an excited crystal have the former mentioned plateau, i. e. quite a rectangular shape, either full or no intensity passes through depending on whether the breadth widens more than the de-tuning or not.

The sharp resonances appear when a standing wave fits into the Silicon crystal i. e. when

$$n \frac{\lambda}{2} = D \tag{1}$$

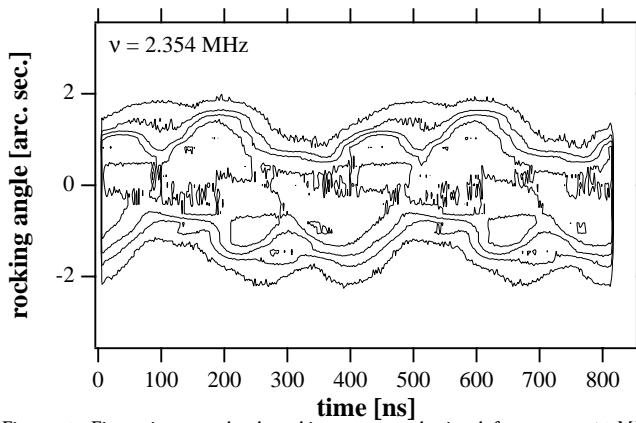


Figure 8: First, time resolved rocking curves obtained from a 2.354 MHz oscillating crystal. The time period is 425 ns. This frequency is close to the transducer resonance and the time distribution is not very sinusoidal. It gives evidence for higher harmonic contamination.

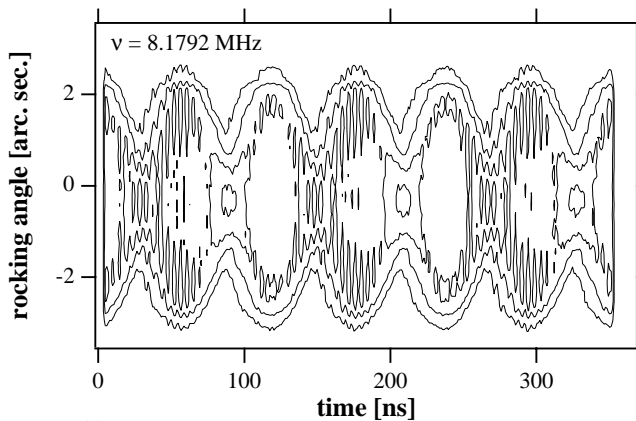


Figure 9: Time resolved spectrum of a crystal vibrating at a sharp resonance with 8.1792 MHz off any transducer resonance. In contrast to figure 8 the oscillation looks sinusoidal corresponding to a clean excitation mode. The time period is 122 ns and seems doubled since the beam integrates over compressed and expanded areas. Note, the spectrum shows the distribution of lattice parameters as a function of time. Highest peak reflectivity is obtained where the rocking curve is narrowest and a central minimum is observed where it is widest.

a half numbered multiple  $n$  of acoustic wavelengths  $\lambda$  equals the total crystal thickness  $D$ . The number of acoustic wavelengths has been calculated with a sound velocity of  $c = 9340$  m/s from the frequency and are indicated on the top axis, fitting perfectly to the observed resonances.

A similar setup has been reconstructed for time resolved experiments using a 2.5 MHz transducer. In addition a surrounding water cooling reducing ultrasonic heating was employed as described in <sup>16</sup> damping further the excited amplitude. A very first intensity distribution as a function of rocking angle, as before, and time is shown in figure (8). These scans are obtained by going to the desired rotation position and measuring stroboscopically the time dependence, proceeding to the next position and so on. Assembled to the matrix from figure (8) they can be cut in time slices as discussed later. The excitation frequency is 2.354 MHz and an oscillation period of 425 ns is easily recognized. The frequency is close to a transducer resonance and the time distribution does not look very sinusoidal. A similar spectrum, displayed in figure (9), off the 3rd transducer harmonics has been taken at 8.1792 MHz, one of the sharp silicon resonances, comparable to those from figure (7). The X-ray energy was 258 keV. The outline looks very clean and harmonic and the amplitude, the maximal rocking width, is about twice as large as in the case before. The time period of 122 ns seems to be doubled because the beam integrates over several wavelengths over compressed and expanded lattice parameters. Time slices can be extracted for different phases of the oscillation and have been assembled to a movie <sup>22</sup>.

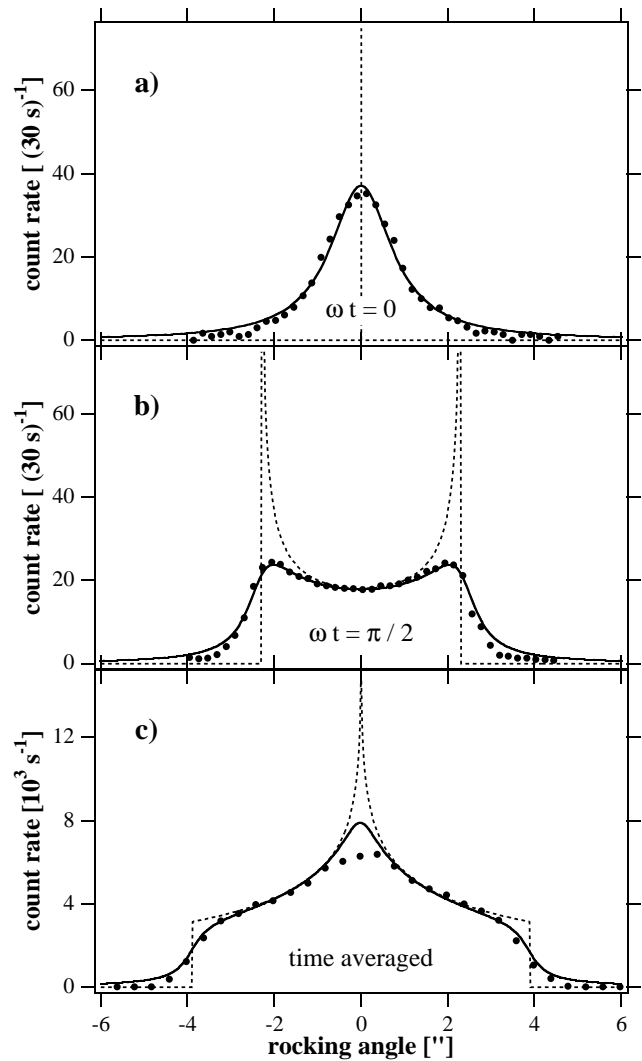


Figure 10: Reflection curves for different snapshots in time, a) and b) and time integrated measurement, c). The upper two curves are obtained by appropriate cuts through figure 9 at moments of narrowest and largest excitations. The black dots are the experimental data while the dashed lines correspond to the mathematical distribution. The latter folded with Lorentzian resolution functions shown by the continuous lines, describe well the behavior of the data.

In particular, a longitudinal standing wave is given by the atomic displacement

$$u(x) = u_0 \sin(\omega t) \sin(k x) \quad (2)$$

from the equilibrium at position  $x$  and time  $t$ ,  $u_0$ ,  $\omega/2\pi$  and  $k$  being its maximal amplitude, frequency and wave number, respectively. In particular, there exist nodes in both space and time, the latter being the moments when the lattice looks undisturbed but is in motion. This corresponds to the times of narrowest rocking widths in the spectrum (9). The moments in between, when the lattice strain blows up to maximal compression in a given volume, or half a period later to maximal compression are called anti nodes. Time slices of the nodes and anti nodes from figure (9) are shown in figure (10a) and (10b), respectively while (10c) shows a time integrated rocking curve, measured independently in a similar setup at 2.55764 MHz and with 100 keV photons. They all differ fundamentally from each other. At these high X-ray energies and reflections used lattice strain is much larger than the natural rocking width of the ideal crystal and the diffraction can be considered dominantly kinematic, representing the distribution of the lattice parameter for the states presented. As already mentioned, at the node in time the lattice looks undisturbed the lattice parameter being distributed by a Dirac  $\delta$ -function, which considerably is enlarged by the resolution function in angle-time space. For all other moments, especially for the anti nodes, the probability  $\rho(u)$  to find a particular atomic amplitude somewhere in the crystal is given by the derivative of the inverse function of (2) and results in

$$\rho(u) = \frac{\partial x}{\partial u} = \frac{1}{k \sqrt{u_t^2 - u^2}} \quad (3)$$

with  $u_t = u_0 \sin(\omega t)$ . We call (3) the inverse circle function since the denominator describes a circle, which has integrable poles at maximum amplitude, vanishes outside and has a local minimum but final value in its center. This function has been adapted to figure (10b) given by the dotted lines, obtained from its convolution with an assumed Lorentzian resolution function, the width fitting best 0.8", the result being the continuous line. The data follow well the same behavior with steep increase at the edges and a dip in the center.

To obtain the time integrated lattice parameter distribution, (3) has to be averaged over one oscillation period, i. e.

$$\bar{\rho}(u) = \frac{2 \omega}{\pi} \int_0^{\frac{\pi}{2\omega}} \rho(u) dt = \frac{2}{\pi k} \int_u^{u_0} \frac{du_t}{\sqrt{(u_t^2 - u^2)(u_0^2 - u_t^2)}} = \frac{2}{\pi k u_0} K\left(\sqrt{1 - \frac{u^2}{u_0^2}}\right) \quad (4)$$

where  $K(q)$  denotes the complete elliptic integral of the first kind with modulus  $q$ <sup>23</sup>. It is characterized by an integrable pole in the center and a logarithmic decrease towards a final value at maximum amplitude and drops there with a step towards zero outside. Again it is plotted in figure (10c) with a dotted line, and also folded with the same resolution Lorentzian as above, represented by the continuous line. The data reflect this behavior, a steep edge forming the shoulder at maximum amplitude at  $\pm 3.5''$  then a further consecutive inflation towards the center. The central deviation from the fit may occur from extinction effects which particularly start playing a role for both this angular position probing for relaxed lattice parameter and the relatively low X-ray energy.

So far, the shape of rocking curves in particular snapshots in time or time integrated have been described and discussed for a sinusoidal oscillation as scanned in figure (9) for a clean silicon resonance. However, the rocking curves from figure (6), analyzed and published earlier<sup>16</sup> do not show at all the characteristic features of the elliptic integral (3) or its convolution. In contrast, they form a large plateau and possess relatively slow decreasing wings as also discussed in the afore mentioned paper. This is now understood qualitatively by the time resolved measurements like the one presented in figure (8). The crystal is not excited by a clean mode but by a series of

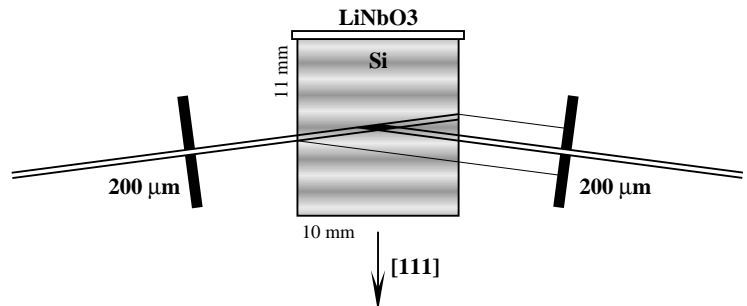


Figure 11: Experimental setup for additional determination of the spatial behavior of the ultrasonic strain field. A pair of 200  $\mu\text{m}$  entrance and exit slits define a small volume in the center of the crystal which can be scanned by translating the sample along its [111] direction, parallel to the sound vectors. Very high X-ray energies of 500 keV have been used to obtain a small scattering angle of  $2\theta = 2.27^\circ$  for the highly resolving Si 555 reflection.

harmonics shifted arbitrarily in phase and destroying the nice nodes in time. At no time is the lattice relaxed, the remaining strain forming the broad plateau value of 100 % after absorption, even in the time average. The oscillations on top of this minimal strain form the wings, highest amplitudes being less probable than the lowers, approaching more smoothly to zero than the step in the elliptic integral.

#### 4. SPACE AND TIME RESOLVED INVESTIGATION OF AN ULTRASONIC FIELD

Results from time resolved experiments on ultrasonically excited crystals have been reported in the previous chapter. There, however, spatial integration over several wavelengths through the whole volume took place as a result of the geometrical setup. The question arose to measure in addition the spatial dependency of the ultrasonic field. Therefore a particular experiment, the setup given in figure (11), was aimed to characterize the ultrasonic standing wave in space and time.

An 11 mm thick silicon crystal has been prepared in a geometry which allows access to both the sound propagation vectors and the scattering vector parallel to the [111] direction. In a perpendicular direction the crystal had a thickness of 10 mm. At 500 keV the scattering angle of the 555 reflection used is  $2.26^\circ$  which gives a beam broadening by the Borrmann triangle through this thickness of 0.4 mm. Entrance and exit slits, each about  $200 \mu\text{m}$  wide were used to limit the scattering volume and thus to probe for the local sound amplitudes as a function of space. Neighboring scans were taken with a 0.5 mm translation of the sample along the sound vector. The resulting scan is shown in figure (12) which is assembled from 13 rocking angle - time scans as seen before. The ultrasound frequency is 2.2399 MHz and the corresponding acoustic wavelength is  $\lambda = 4.17 \text{ mm}$ . A broad rocking curve at given times reflects a maximum sound amplitude, while a narrow one relates to the strain free zero transition. Nodes in space are expected with a periodicity of  $\lambda/2$  and indeed they are observed by the lower amplitudes around 2.4 mm and 5.5 mm. The ordinate position 0 is roughly 1 mm below the surface carrying the transducer, and positive space coordinates are further away from the exciting surface. Note, that no nice wave pattern is formed up to the ordinate 2 mm, neither in space nor in time: In particular no well defined phases of the strain amplitude can be identified in the ordinate range of say

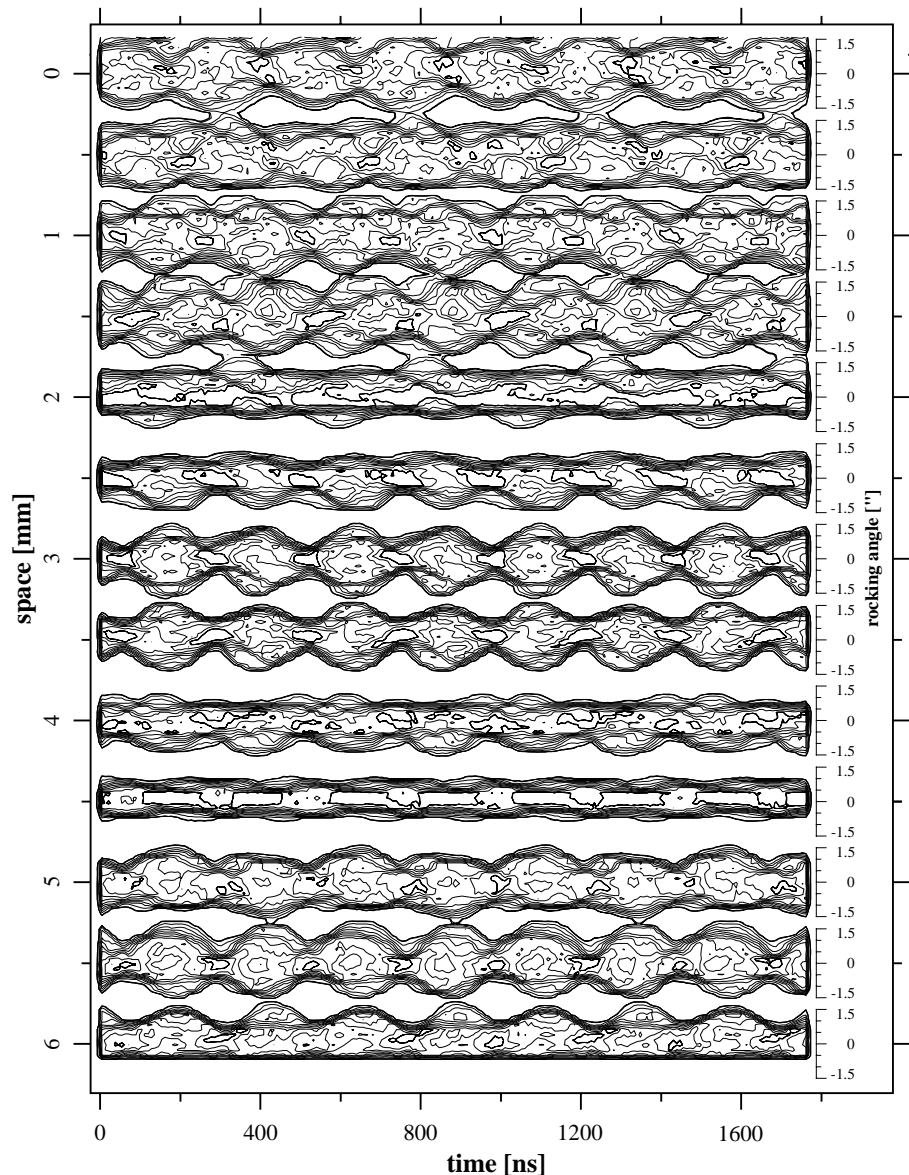


Figure 12: Intensity distribution as a function of rocking angle (right), time (bottom) and space (left) scale. Each row represents a spectrum as detailed in figures 8 or 9. The transducer surface is located -1 mm beyond the uppermost spectrum. Spatial nodes of the standing wave are recognized by smaller amplitudes around 2.25 mm and 4.5 mm and temporal nodes occur when the intensity distribution in a row is narrowest. The figure demonstrates a very distorted near field close to the transducer where a spatial node is missing and the sound spectrum seems to be established by higher harmonics. Time phase and spatial nodes improve in the deeper volume.

up to 2 mm. In contrast, for higher values a clean wave pattern with distinguished areas of maximum amplitudes and for nodes is seen in both space and time. Another indication for an evolution of a highly disturbed wave near the transducer towards a plane wave in the volume is the contribution of harmonics, revealed from the asymmetry of the rocking angle - time scans. Although the wave becomes locally plane the individual time scans show an average over compressed and expanded crystal regions. This may be a hint that the crystal macroscopically shows sound figures as we observed them in a neutron topography<sup>24</sup> because diffraction integrates along quite a large volume perpendicular to the wave vector. If sound figures would exist the beam could see compressed lattice parameters on the left at the same time when they were expanded on the right half of the crystal, for example.

## 5. CONCLUSION

Time resolved investigation of ultrasonically excited crystals performed on the high resolution 3-axes diffractometer at the high energy beamline ID15A have been presented in both detection techniques and results.

The detector system can run in two modes, the detector mode, independent from the synchrotron source and in the synchrotron mode. In both cases full energy resolution of the germanium detector is exploited. The former mode uses classically the raising edge of the detector signal itself while the second synchronizes the jittered output pulse to the bunch clock, i. e. the time when an X-ray flash appears from a single bunch in N-bunch mode. Time resolutions of 20 ns and about 200 ps, respectively, have been achieved and are standardly available, together with the high resolution high energy X-ray diffractometer, mainly for rapidly repeatable processes in solid state physics.

The effect of ultrasound on a perfect silicon crystal has been studied. Classical, time integrated measurements show the broadening of the reflection curve due to the strain induced. The integrated intensity gain raised up to a factor of 50 towards the unexcited sample which certainly is a good criteria for choosing such a tunable device as an adaptable monochromator. A development in this direction has been started for the topography beamline ID19<sup>25</sup>. Further more the investigation of the ultrasonic field itself is a major topic of the present work. Atomic amplitudes up to 210 Å peak to peak have been obtained with the current setup and the values are directly deduced from the broadening of the rocking curve. The time resolved diffraction gives detailed insight to the quality of the ultrasonic excitation. Thus resonances close to the transducer resonance are composed by a variety of harmonic excitation and no clean diffraction pattern is obtained. Further tests like a deviation from the sinusoidal towards a rectangular excitation have been performed and are related directly to the diffraction pattern. The best sinusoidal excitations can be stimulated off the transducer harmonics when a standing wave fits into the silicon crystal. There the exciting amplitude is small but the resonance effect leads to the largest elongation observed. The time resolved experiments also give a better understanding of previously measured reflection curves and we could come to the conclusion that not always clean modes were excited where assumed in literature.

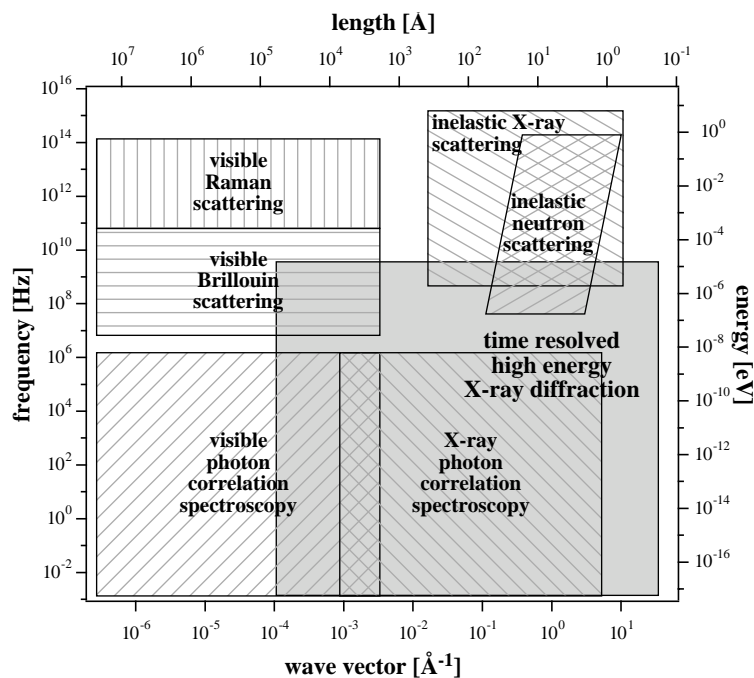


Figure 13: The regions of wavevector-energy space covered by various techniques are indicated. The time resolved high energy X-ray diffraction would provide a unique probe in a previously inaccessible region.

## 6. OUTLOOK

Time resolved X-ray diffraction experiments clearly play a strongly increasing role in solid state physics. On one hand new optical elements like beam choppers are needed for example to replace mechanical devices like those employed on ID9<sup>18</sup> separating the single bunch from hybrid mode from the 1/3 multibunch fill. Herefore ultrasonically excited crystals are a potential starting point. The investigation of optical properties like the ray trace in the Borrmann triangle have been started and are important parameters to design the desired time structures and contrasts. On the other hand, the time window

accessible by the introduced method together with the momentum transfer  $Q$  obtainable by high energy X-rays fill an important gap in probing dynamic excitations. Figure (13) <sup>26</sup> shows the wavevector-energy space covered by various techniques. The area accessible by the presented time and momentum resolution is indicated and overlaps with the gap between the techniques of X-ray photon correlation spectroscopy and inelastic neutron scattering. Of course, our technique does not work in thermodynamic equilibrium but time constants could be measured as a response to any excitation which then relate by the fluctuation-dissipation theorem to the same physics as obtained by other methods. For example, the phase transition in strontium titanate could be driven by an ultrasonic wave measuring directly the relaxation as a function of the phase of the distortion. Further ultrasonic waves are employed classically for the investigation of diffusion processes with the model of the anharmonic oscillator <sup>27,28</sup>. The well known example is bcc iron with interstitial positions on the three face centers which might be occupied by a diffusing impurity like carbon or nitrogen. A compressional wave causes lattice strain splitting energy levels of these originally three equivalent positions, which leads to relaxation by diffusion from the higher to the lower energetic positions. Then stimulated excitation equal with the hopping frequency of the atoms leads into a resonance peak in the absorption spectrum of the ultrasonic wave. If now, the occupancy of the interstitial sites could be observed by time resolved X-ray diffraction, not only the relaxation time but also the relaxation mechanism itself would be measured. Relaxation times of the mentioned example at 150°C would lie in the MHz range, perfectly accessible by our technique. The only question might be a tiny signal since thermal activation will work against the relaxation of the occupation numbers.

## 7. ACKNOWLEDGMENTS

The authors would like to thank Uwe Bergmann for his helpful introduction into time resolved detection, not only by discussion but also by manual help on the beamline.

## 8. REFERENCES

1. G. W. Fox, P. H. Carr, "The effect of piezoelectric oscillation on the intensity of X-ray reflections from quartz" *Physical Review*, **37**: p. 1622-1625, 1931.
2. T. F. Parkinson, M. W. Moyer, "Modulation of diffracted neutrons with a piezoelastic crystal" *Nature*, **211**: p. 400-401, 1966.
3. A. R. Mkrtchyan, M. A. Navasardian, R. G. Gabrielyan, L. A. Kocharian, "Controlled focusing of the Å wavelength radiation in case of the ultrasound modulation or temperature gradient" *Solid State Communications*, **59**(3): p. 147-149, 1986.
4. R. Hock, T. Vogt, J. Kulda, Z. Mursic, H. Fuess, A. Magerl, "Neutron backscattering on vibrating silicon crystals - experimental results on the neutron backscattering spectrometer IN10." *Zeitschrift für Physik*, **B 90**: p. 143-153, 1993. 93HO125
5. A. Remhof, K.-D. Liß, A. Magerl, "Neutron diffraction from sound excited crystals" *Nuclear Instruments and Methods*, **391**(A): p. 485-491, 1997.
6. E. Zolotoyabko, I. Polikarpov, "Determination of crystal imperfection by X-ray diffraction in a strong acoustic field" *Journal of Applied Crystallography*, (25): p. 88-91, 1992.
7. E. Zolotoyabko, B. Sander, "X-ray diffraction profiles in strained crystals undergoing ultrasonic excitation. The Laue case" *Acta Crystallographica*, **A**(51): p. 163-171, 1995.
8. S. D. LeRoux, R. Colella, R. Bray, "X-Ray Diffraction Studies of Acoustically Amplified Phonon Beams" *Physical Review Letters*, **35**(4): p. 230-234, 1975.
9. V. L. Nosik, "Dynamical X-ray Focusing under Conditions of the X-ray Acoustic Resonance: I. Focusing in Perfect Crystals" *Crystallography Reports*, **39**(4): p. 526-534, 1994.
10. S. Kikuta, T. Takahashi, S. Nakatani, "High frequency time modulation of the X-ray beam diffracted from a LiNbO<sub>3</sub> crystal by surface acoustic waves." *Japanese Journal of Applied Physics*, **23**(4): p. L193-L194, 1984.

11. R. Hock, K.-D. Liss, A. Magerl, O. G. Randl, A. Remhof, "Neutron storage in a longitudinally vibrating silicon crystal" *Journal of Applied Crystallography*, **submitted**, 1997.
12. A. R. Mkrtchyan, M. A. Navasardyan, L. A. Kocharyan, K. G. Galoyan, R. G. Gabrielyan, O. A. Unanyan, "Double modulation of X radiation by high- and low-frequency acoustic waves" *Soviet Technical Physics Letters*, **12**(12): p. 629-631, 1986.
13. A. R. Mkrtchyan, M. A. Navasardyan, L. A. Kocharyan, V. K. Mirsoyan, O. A. Unanyan, K. T. Airapetyan, "Modulation of synchrotron radiation by acoustic oscillations" *Izvestiya Akademii Nauk Armyanskoi SSR. Fizika*, **21**(6): p. 326-330, 1986.
14. R. Tucoulou, I. A. Schelokov, D. V. Roshchupkin, M. Brunel, L. Ortega, P. Cevalier, "Diffraction of a focused X-ray beam by surface acoustic waves" *Optics Communications*, **118**: p. 175-180, 1995.
15. B. Waibel, K.-D. Liss, A. Magerl, T. Hansen, "Ultrasound excited crystals as switchable neutron mirror". Experimental Report, Institut Laue Langevin, 1998.
16. K.-D. Liss, A. Magerl, A. Remhof, R. Hock, "Ultrasound induced gradient crystals observed by high energy X-rays" *Acta Crystallographica*, **A**(53): p. 181-186, 1997.
17. K.-D. Liss, A. Royer, T. Tschentscher, P. Suortti, A. P. Williams, "On high resolution reciprocal space mapping with a triple crystal diffractometer for high energy X-rays" *Journal of Synchrotron Radiation*, **5**: p. 82-89, 1998.
18. M. Wulff, F. Schotte, D. Bourgeois, F. Zontone, S. Techert, G. Naylor, K. Scheidt, P. A. Anfinrud, K. Moffat, G. A. Mourou, "Synchrotron-based ultrafast X-ray scattering: beamline ID09 at the European Synchrotron Radiation Facility" *Proceedings of SPIE*, **3451**, 1998.
19. K.-D. Liss, A. Magerl, R. Hock, A. Remhof, B. Waibel, "Towards a new (Q, t) regime by time-resolved X-ray diffraction: ultra-sound excited crystals as an example" *Europhysics Letters*, **40**(4): p. 369-374, 1997.
20. K.-D. Liß, "Ultrasonic excitations studied by X-rays". [http://www.esrf.fr/exp\\_facilities/id15a/science/usw.html](http://www.esrf.fr/exp_facilities/id15a/science/usw.html): 1998.
21. K.-D. Liß, "Strukturelle Charakterisierung und Optimierung der Beugungseigenschaften von  $\text{Si}_{1-x}\text{Ge}_x$  Gradientenkristallen, die aus der Gasphase gezogen wurden". Dissertationsschrift, Rheinisch Westfälische Technische Hochschule Aachen, 27 Oktober 1994. [http://www.esrf.fr/exp\\_facilities/id15a/theses/DissLiss/Zusammenfassung.html](http://www.esrf.fr/exp_facilities/id15a/theses/DissLiss/Zusammenfassung.html)
22. K.-D. Liß, "The X-ray movie page". 1998. [http://www.esrf.fr/exp\\_facilities/id15a/science/SPIE98/index.html](http://www.esrf.fr/exp_facilities/id15a/science/SPIE98/index.html)
23. I. S. Gradshteyn, I. M. Ryzhik, "*Table of integrals, series, and products*" Academic Press: New York. , 1980.
24. A. Remhof, "Neutronen- und Röntgenstreuung an Idealkristallen im Ultraschallfeld". Diplomarbeit, Ruhr Universität Bochum, Februar 1996. 90LI2013
25. S. Köhler, "Charakterisierung eines mit Ultraschall angeregten Kristalls als Monochromator in Bragg-Geometrie". Diplomarbeit, Julius-Maximilian-Universität Würzburg, Juni 1998.
26. S. Dierker, "X-Ray Photon Correlation Spectroscopy at the NSLS" *NSLS Newsletter*, , July 1995. <http://www.nsls.bnl.gov/Intro/Newslet/Jul95/speckle.html>
27. B. S. Berry, A. S. Nowick, "Anelasticity and internal friction due to point defects in crystals" in "*Physical Acoustics*", W. P. Mason, Editor. Academic Press: New York and London. p. 1-42, 1966.
28. A. S. Nowick, B. S. Berry, "*Anelastic relaxation in crystalline solids*" Academic Press: New York and London. , 1972.